Experimental study using infrared thermography on the convective heat transfer of a TGV brake disc in the actual environment,

Monica Siroux, Souad Harmand, Bernard Desmet

Experimental study using infrared thermography on the convective heat transfer of a TGV brake disk in the actual environment

Monica Siroux
Souad Harmand
Bernard Desmet
Université de Valenciennes et du Hainaut-Cambrésis
Laboratoire de Mécanique et Energétique
Le Mont Houy, F-59313
Valenciennes Cedex 9
France
E-mail: Monica.Siroux@univ-valenciennes.fr

Abstract. We present an experimental identification of the local and mean Nusselt number from a rotating TGV brake disk model in the actual environment and exposed to an air flow parallel to the disk surface. This method is based on the use of a heated thermally thick disk combined with the technique of temperature measurement by infrared thermography. The local and mean convective heat transfer coefficient from the disk surface is identified by solving the steady state heat equation by a finite difference method using the experimental temperature distribution as boundary conditions. The experimental setup is constituted of a model disk with all the representative parts of the actual TGV brake system. The disk and its actual environment are inside a wind tunnel test section, so that the rotational disk speed and the air flow velocity can be varied. Tests were carried out for rotational speeds ω between 325 and 2000 rpm (rotational Reynolds number Re between 88,500 and 545,000), and for an air flow velocity U ranging between 0 and 12 $m \cdot s^{-1}$ (air flow Reynolds number Re_0 between 0 and 153,000). [DOI: 10.1117/1.1481896]

Subject terms: infrared thermography; heat convection; Nusselt number; brake disk; brake environment.

Paper 010232 received July 5, 2001; revised manuscript received Jan. 17, 2002; accepted for publication Jan. 31, 2002.

1 Introduction

High energy train braking implies a significant brake disk temperature increase (local temperature ranging between 500 and 1000°C) that can damage the disk. The railway equipment industry is therefore trying to find new TGV brake disk system cooling strategies, such as a heat pipe disk.[1] One solution consists in conceiving a specific design that directs the air flow produced by the train displacement toward the disk. The air flow produced by the train displacement that arrives on the disk is very weak. Consequently, it is necessary to analyze the influence of the air flow cooling on the convective heat transfer on the TGV brake disk. This study presents an experimental determination of the local and mean Nusselt number from a rotating TGV brake disk model in the actual environment that is submitted to an air flow parallel to the disk surface.

The convective heat transfer from a simple disk rotating in still air, regardless of whether the temperature is uniform or not, has been described by many authors. Von Karman[2] studied the flux induced by a rotating disk. Rotation transmits tangential and radial velocity components to the fluid close to the surface. For a disk with a given outer radius, the fluid is rejected towards its periphery, which causes an axial fluid flow toward the disk. The movement produced by a rotating disk is divided into three modes: laminar, transitional, and turbulent. Gregory, Stuart, and Walker[3] sought to establish how laminar flow loses its stability in the vicinity of a rotating disk. Two critical radii were obtained, separating the three modes of the flow. In the central zone to the radius R_c the flow is purely laminar, and beyond the radial position R_t it is entirely turbulent. The rotational Reynolds numbers connected to these two positions of instability and transition are given by:

$$Re_c = \omega \cdot R_c^2 / \nu_a = 1.82.10^5 \quad \text{(instability)} \tag{1}$$

$$Re_t = \omega \cdot R_t^2 / \nu_a = 2.82.10^5 \quad \text{(transition)}. \tag{2}$$

Other authors, like Cobb and Saunders,[4] Wagner,[5] Sparrow and Gregg,[6] Richardson and Saunders,[7] Oehlbeck and Erian,[8] Hartnett,[9] and Dorfman[10] studied the heat transfer of a rotating disk in still air. Dorfman suggests, for a temperature distribution $T = T_\infty + cr^n$, a correlation giving the local Nusselt number as function of the rotational Reynolds number:

$$Nu = 0.22(n+2)^{1/2} Re^{0.5} \quad \text{(laminar flow)} \tag{3}$$

$$Nu = 0.0169(n+2.6)^{0.2} Re^{0.8} \quad \text{(turbulent flow)}. \tag{4}$$

Some studies give the evaluation of the heat transfer coefficient when both rotational and superimposed air flow parallel to the disk surface are combined. De Vere[11] presents a correlation when air flow velocity and rotational speed of the disk are linked by the relation $U = \omega R$. De Vere showed that the heat transfer on the disk is dominated by the main flow of air more than by the secondary rotational flow. In the case of a rotating TGV brake disk exposed to an air flow parallel to the disk surface, Watel[12] put forward experimental results in concordance with those obtained by De Vere.

 0091-3286/2002/$15.00

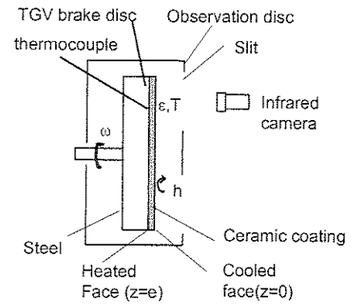

Fig. 1 Schema of the TGV brake disk.

2 Experimental Procedure and Apparatus

2.1 *Procedure for the Determination of the Local Convective Heat Transfer Coefficient*

The local convective heat transfer coefficient measurement technique consists of using a thermally thick wall combined with the surface temperature measurement by infrared thermography and the numerical resolution of the steady state heat equation. The thermally thick wall is composed of a steel disk and a ceramic coating. The steel part of the disk is heated by electric resistances and its role is to homogenize the temperature inside the thermally thick wall. The ceramic coating is cooled by the air flow (Fig. 1). Due to the low conductivity of ceramics, the variations of the convective heat transfer coefficients h along the disk radius r are related to the variations of the surface temperature along the radius, which can be detected by infrared thermography.

The numerical resolution of the steady state heat equation gives access to the local convection coefficient on the disk. The steady state heat equation for the axisymmetric problem inside the ceramic part of the disk is:

$$\frac{\partial^2 T}{\partial r^2} + \frac{1}{r}\frac{\partial T}{\partial r} + \frac{\partial^2 T}{\partial z^2} = 0. \tag{5}$$

The boundary conditions in this work are: for $z = 0$, $T(r,0)$ is given by the infrared camera and for $z = e$, $T(r,e)$ is given by the thermocouples. A finite difference method has been used to solve these equations. The local heat flux from the disk surface can be deduced by using the thermal balance on the disk surface:

$$\varphi_{conduction} = \varphi_{convection} + \varphi_{radiation} \tag{6}$$

with

$$\varphi_{conduction} = \lambda_c \left(\frac{\partial T}{\partial z}\right)_{z=0}$$

local conductive heat flux

$$\varphi_{convection} = h[T(r,0) - T_\infty]$$

losses by convection

$$\varphi_{radiation} = \frac{\epsilon}{1-\epsilon}[\sigma \cdot T^4(r,0) - J]$$

losses by radiation.

Then local and mean Nusselt numbers are deduced

$$Nu = \frac{h \cdot r}{\lambda_a} = \frac{\lambda_c \left(\frac{\partial T}{\partial z}\right)_{z=0} - \frac{\epsilon}{1-\epsilon}[\sigma T^4(r,0) - J]}{T(r,0) - T_\infty} \frac{r}{\lambda_a} \tag{7}$$

$$Nu_m = \frac{h_m R_2}{\lambda_a} = \frac{2R_2}{R_2^2 - R_1^2} \frac{1}{T - T_\infty} \int_{R_1}^{R_2} (T - T_\infty) Nu \, dr. \tag{8}$$

The surface temperature gradient $(\partial T/\partial z)_{z=0}$ is given by the numerical solution of the heat equation. The disk surface temperature $T(r,0)$ and the disk emissivity ϵ are obtained by infrared thermography, and the temperature of the flow T_∞ is measured by a thermocouple. The disk radiosity J is estimated from the radiative exchange balance between the disk surface and its surrounding[13,14]:

$$J = \frac{\epsilon \sigma T^4(r,0) + (1-\epsilon)\epsilon_s \sigma T_s^4}{1 - (1-\epsilon)(1-\epsilon_s)} \tag{9}$$

$\epsilon_s = 0.65$ and T_s are the emissivity and the temperature of the aluminum wall of the test section located close to the TGV disk, respectively.

2.2 *Experimental Setup*

The experimental setup comprises the TGV model disk on scale 0.617 and its actual environment. The TGV model disk is made of steel (inner radius $R_1 = 51$ mm, outer radius $R_2 = 197$ mm, and thickness $e' = 26$ mm) and covered by a ceramic coating obtained by plasma projection (conductivity $\lambda_C = 0.65\ W\,m^{-1} \cdot K^{-1}$, and thickness $e = 1.7$ mm). To simulate the energy dissipation by friction, the steel part of the disk is equipped with eight electric resistances. All the representative parts of the actual TGV brake system (flanges, pads, brake lining holders, cylinder, and brake rods) are found around the disk (Figs. 2 and 3).

The TGV model disk and its actual environment are installed inside the wind tunnel test section with aluminum walls (dimensions 1037×671×225). One of the wind tunnel walls is equipped with an observation disk (diameter 470 mm), which comprises two slits (dimensions 107×13 mm), making it possible to visualize the surface temperature by infrared thermography in line scanning mode. The rotational disk speed varies from 300 to 2000 rpm using an engine at variable speeds, and the relative error on the rotational speed measurement is 0.5%. The air flow velocity varies from 0 to 12 $m\,s^{-1}$ using a blower and is measured by a Pitot tube placed in the test section casing. A convenient velocity distribution is obtained thanks to a honeycomb at the inlet of the wind tunnel.

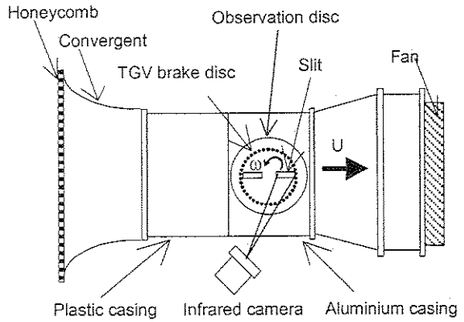

Fig. 2 Experimental setup.

To determine the local Nusselt number, the temperature of the flow, the temperature at the ceramic/steel interface, the temperature of the aluminum wall of the test section, and the disk temperature surface, are measured. The temperature of the flow T_∞ is measured by a K-type thermocouple placed inside the test section, and the absolute error on T_∞ can be estimated at $\Delta T_\infty = \pm 0.3$ K. The temperature at the ceramic/steel interface is measured by two K-type thermocouples placed at 70 and 170 mm, respectively, from the disk axis, and the absolute error on this temperature is $\Delta T = \pm 0.3$ K. The temperature of the aluminum wall of the test section T_s is measured by a K-type thermocouple and the absolute error on this temperature is $\Delta T_s = \pm 0.3$ K. The disk surface temperature is obtained by infrared thermography.

2.3 *Disk Surface Temperature Measurements Using Infrared Thermography*

The TGV disk surface temperature T is obtained from the thermal level measured by a short wave wide band infrared thermography camera (AGEMA 900 SW/TE, $\lambda = 2$–5.4 μm). The infrared camera equipped with a $20 \times 12.5°$ lens is installed in front of the TGV brake disk so that its optical axis is merged with the disk rotational axis. In this way the temperature distribution is obtained along a radius of the disk surface with a line acquisition frequency of 3472 Hz (Fig. 2).

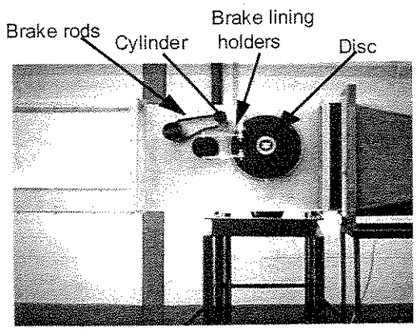

Fig. 3 View of the experimental setup.

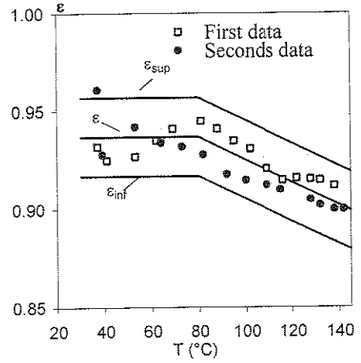

Fig. 4 Black paint emissivity.

The thermal level I_m, determined thanks to the infrared camera, takes the thermal level of the brake disk surface $I(T)$, the thermal level of the environment $I(T_{\text{env}})$, the atmospheric transmission τ, and thermal level of the atmosphere $I(T_{\text{atm}})$ into account[15,16]:

$$I_m = \tau \cdot \epsilon \cdot I(T) + \tau \cdot (1-\epsilon) \cdot I(T_{\text{env}}) + (1-\tau) \cdot I(T_{\text{atm}}). \quad (10)$$

The thermal level of the brake disk surface $I(T)$ is a function of the disk surface temperature T through the calibration curve $I(T) = f(T)$ obtained by using a black body (AGEMA BB 400-3) of emissivity equal to 0.99 ± 0.01. To maximize the disk thermal emission, when compared to the thermal level of the environment $I(T_{\text{env}})$, the disk surface was covered with a high emissivity black paint supposed to be an opaque, lambertian, and gray surface in emission and reflection.

To determine the black paint emissivity, two measurements of I are carried out: the first one on the black paint disk surface (giving I_m) and the second one on a lambertian aluminum surface (giving I_a):

$$I_a = \tau I(T_{\text{env}}) + (1-\tau) I(T_{\text{atm}}). \quad (11)$$

The black paint emissivity is deduced by using Eqs. (10) and (11):

$$\epsilon(T) = \frac{(I_m - I_a)}{\tau I(T) - I_a + (1-\tau) I(T_{\text{atm}})}. \quad (12)$$

While the disk surface temperature T and atmospheric temperature T_{atm} are measured by thermocouples, the calibration curve leads to the identification of the thermal levels $I(T)$ and $I(T_{\text{atm}})$. It is then possible to identify the black paint emissivity in the spectral band of the camera.[17] Figure 4 shows the black paint emissivity values obtained for several different temperatures. It can be seen that for a temperature ranging between 30 and 80°C (which is the temperature range used for the tests), the black paint emissivity is $\epsilon = 0.93 \pm 0.02$. Equations (10) and (11) are therefore used to deduce the disk thermal level $I(T)$:

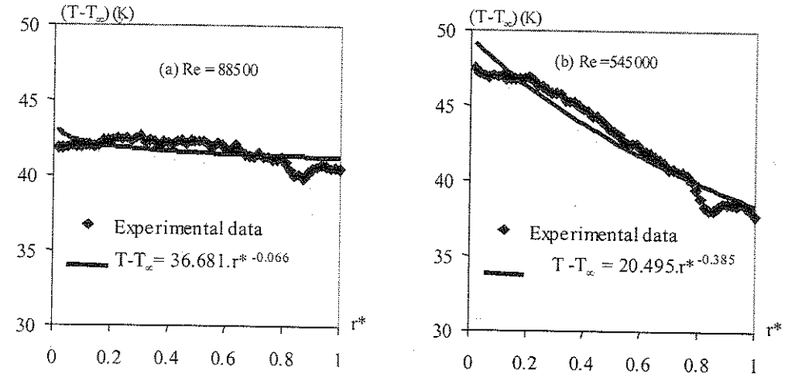

Fig. 5 Experimental temperature evolution as a function of the dimensionless radius: (a) Re=88,500 and (b) Re=545,000.

$$I(T) = \frac{I_m - (1-\epsilon) I_a - \epsilon(1-\tau) I(T_{\text{atm}})}{\tau \epsilon}. \quad (13)$$

The calibration curve is then used to obtain the disk surface temperature. The uncertainty obtained on the disk temperature T is $\Delta T = \pm 0.90$ K.

3 Results of the Test on the Convective Heat Transfer

The convective heat transfer experiments were carried out for rotational speeds ω between 325 and 2000 rpm (rotational Reynolds number $\text{Re} = \omega R^2/\nu_a$ between 88,500 and 545,000), so as to obtain laminar and turbulent flow on the disk, and for air flow velocity U ranging between 0 and 12 m s^{-1} (air flow Reynolds number $\text{Re} = UR/\nu_a$ between 0 and 153,000). These measurements aim to show the influence of the air flow cooling on the convective heat transfer on the TGV brake disk.

3.1 *Temperature Profiles*

Dorfman[10] showed that it is essential to take the influence of a radial temperature distribution on the disk into account when evaluating the local heat transfer coefficient. This is why the experimental temperature evolution $T - T_\infty$ is presented as a function of the dimensionless disk radius $r^* = (r - R_1)/(R_2 - R_1)$. Figure 5(a) shows the experimental temperature evolution for rotational speed $\omega = 325$ rpm (Re = 88,500) and Fig. 5(b) shows the experimental temperature evolution for rotational speed $\omega = 2000$ rpm (Re = 545,000). The experimental temperature evolution on the disk surface is represented by a power law of the type $T - T_\infty = c r^{*n}$, where exponent n is a function of the experimental conditions. In our case, n varies between -0.066 and -0.385.

It can be seen [Figs. 5(a) and 5(b)] that the disk temperature decreases with the dimensionless radius r^*. This reduction is due to the increase of the convective heat transfer for large dimensionless radius r^* values. A slight fall in temperature profile around the dimensionless radius r^* 0.8 to 0.9 is also noticed. For these values of the radius r^*, the brake shoe print can be observed on the disk surface. These frictions damaged the black painting that cover the disk and led to a reduction of the disk emissivity surface and thus of the measured surface temperature.

3.2 *Contribution of the Radiative Losses Compared to the Convective Losses*

Figures 6(a) and 6(b) show the contribution of the radiative losses compared to the convective losses [Eq. (6)]. For a weak rotational speed value [Fig. 6(a): $\omega = 325$ rpm, Re = 88,500], the radiative losses are very significant (on average 44%) if the rotating disk is in still air ($U = 0$, $\text{Re}_0 = 0$). It is thus necessary to take them into account in the calculation of the heat transfer coefficient. However, for a rotating disk exposed to an air flow, these losses decrease considerably (they are about 6% for $U = 12$ m s^{-1} $\text{Re}_0 = 153{,}000$). For a high rotational speed value [Fig. 6(b): $\omega = 2000$ rpm, Re = 545,000], the radiative losses are very weak (in the order of 6%) and thus it is less important to take them into account.

3.3 *Local Nusselt Number*

The local Nusselt number is plotted as a function of the dimensionless radius r^* [Figs. 7(a) and 7(b)]. Figure 7(a) shows the local Nusselt number for rotational speed $\omega = 325$ rpm (Re = 88,500) and for air flow velocity U ranging from 0 to 12 m s^{-1} ($0 \leqslant \text{Re}_0 \leqslant 153{,}000$). Figure 7(b) presents the local Nusselt number for rotational speed $\omega = 2000$ rpm (Re = 545,000) and for air flow velocity U ranging from 0 to 12 m s^{-1} ($0 \leqslant \text{Re}_0 \leqslant 153{,}000$). Dorfman's results on the rotating disk in still air ($U = 0$ m s^{-1}) are also plotted.

For a laminar flow on the rotating disk in still air, our experimental results are in concordance with Dorfman's correlations [Fig. 7(a)]. For a higher rotational Reynolds number, corresponding to a turbulent flow on the rotating disk in still air [Fig. 7(b)], our results are in good agreement with Dorfman's correlations for a dimensionless radius lower than $r^* = 0.5$. For values over $r^* = 0.5$, corresponding to the friction zone, our experimental results are higher than Dorfman's predictions. The actual environment of the brake disk probably modifies significantly the flow

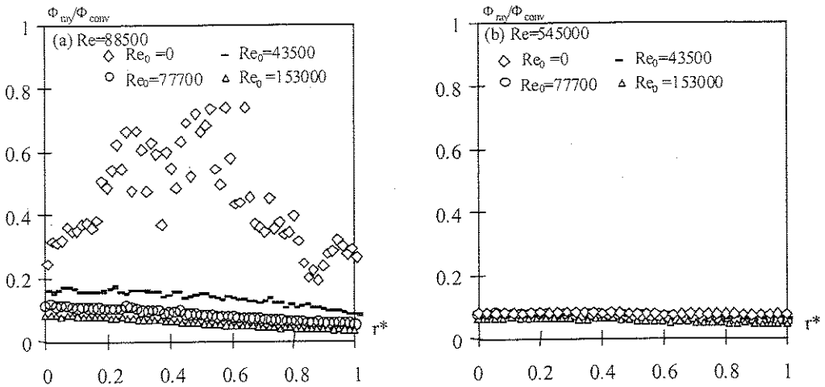

Fig. 6 Contribution of the radiative losses compared to the convective losses: (a) Re=88,500 and (b) Re=545,000.

structure by increasing turbulence and thus heat transfer from the disk. When rotation and air flow velocities are combined, one notices that for a low rotational speed ω=325 rpm (Re=88,500), the influence of the air flow velocity on the convective exchange is significant [Fig. 7(a)]. Indeed, the passage of Re_0=43,500 (U=3 m s^{-1}) to Re_0 =77,700 (U=6 m s^{-1}) involves an increase of the peripheral Nusselt number of 33%. In the same way, the passage of Re_0=77,700 (U=6 m s^{-1}) to Re_0=153,000 (U =12 m s^{-1}) involves an increase of the peripheral Nusselt number of 40%.

In Fig. 7(b), when rotation and air flow velocity are combined for a high rotational speed ω=2000 rpm (Re =545,000), it can be seen that the influence of the air flow on the Nusselt number becomes less significant. The passage of Re_0=43,500 (U=3 m s^{-1}) to Re_0=77,700 (U =6 m s^{-1}) involves an increase of the peripheral Nusselt number of 16.7%, whereas the passage of Re_0=77,700 (U=6 m s^{-1}) to Re_0=153,000 (U=12 m s^{-1}) involves an increase of the peripheral Nusselt number of only 25%.

3.4 *Mean Nusselt Number*

The evolution of the mean Nusselt number in the study zone as a function of the Reynolds number is plotted in Figs. 8(a) and 8(b). For a rotating disk in still air [Fig. 8(a)], the mean of our experimental results is higher than that of Dorfman (19% higher for a laminar flow and 17% higher for a turbulent flow). This increase can be attributed to the presence of the actual disk environment. When both rotational and superimposed air flows are combined [Fig. 8(b)], one notices that the air flow velocity influence on the mean Nusselt number is significant for low rotational speeds and decreases for high rotational speeds. This shows that for a low rotational speed, the convective heat exchange is dominated by the air flow, and that for a high rotational speed, the convective heat exchange is dominated by rotation.

3.5 *Comparison with the Correlation Given by De Verre for U= R ω Configuration*

When a TGV brakes, rotational speed and air flow velocity are connected by the relation $U=R_w\omega$, where R_w is the

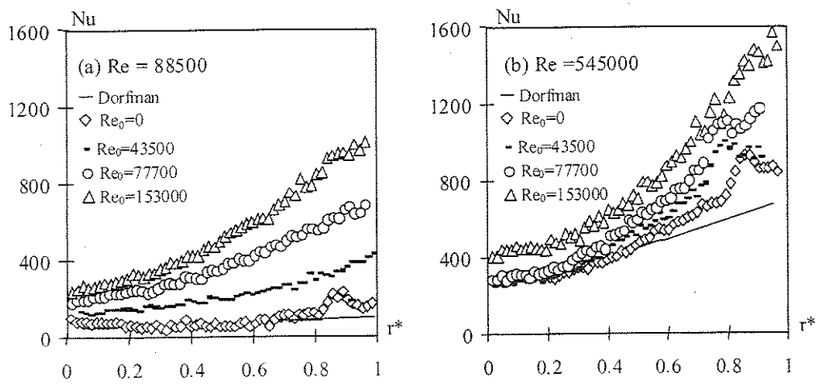

Fig. 7 The local Nusselt number as a function of the dimensionless radius: (a) Re=88,500 and (b) Re=545,000.

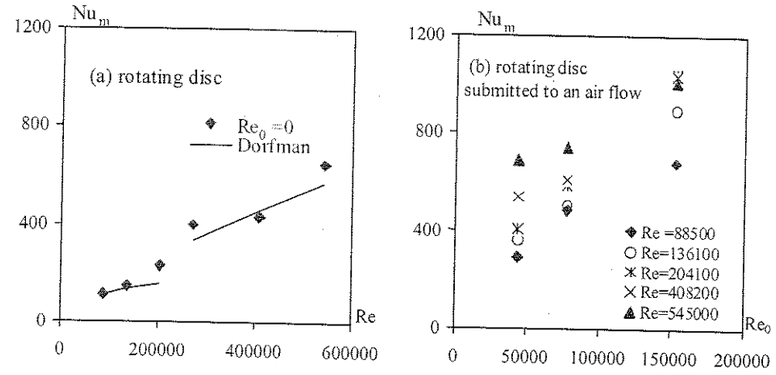

Fig. 8 The mean Nusselt number as a function of the Reynolds number: (a) rotating disk and (b) rotating disk submitted to an air flow.

wheel radius. This is why our results and the correlation given by De Vere[11] for a $U=R\omega$ configuration are compared in Fig. 9 (rotational speed ω ranging between 386 to 560 and air flow velocity U ranging between 8 and 12 m s^{-1}). For a weak dimensionless radius $r^*<0.4$, our test results are close to those given by De Vere. On the contrary, for significant dimensionless disk radius $r^*>0.4$, our values are much higher than those of De Vere. This difference can be explained by the influence of the TGV disk's actual environment (our experimental configuration includes the TGV disk actual environment, which is not the case for the study undertaken by De Vere) associated with the nature of temperature distribution (De Vere's tests were carried out on an isothermal disk, whereas in our case the disk temperature distribution is similar to a power law $T=T_\infty + cr^{*n}$).

4 Conclusion

This work describes an experimental study used to determine the local and mean Nusselt number from a thermally thick TGV brake disk placed in its actual environment. The experimental method uses a thermally thick wall combined with the temperature measurement by infrared thermography. The local convective heat transfer coefficient from the disk surface is identified by solving the steady state heat equation by the finite difference method using the experimental temperature distribution for boundary conditions.

The experimental setup is constituted of a model disk with all the representative parts of the actual TGV brake system. The model disk and its actual environment are inside the wind tunnel test section, so that the rotational disk speed and air flow velocity can be varied. The brake disk surface temperature is identified thanks to a short wave infrared thermography camera. Tests are carried out for rotational speeds ω from 325 to 2000 rpm (rotational Reynolds number Re between 88,500 and 545,000) so as to obtain laminar and turbulent flow on the disk, and for air flow velocity U ranging from 0 to 12 m s^{-1} (air flow Reynolds number Re_0 between 0 and 153,000).

For a rotating disk in still air, the comparison of our experimental results with those of the bibliography shows that the presence of the actual environment leads to an increase of the mean heat transfer coefficient. When both rotational and superimposed air flow parallel to the disk surface are combined, the experimental results give rise to the following conclusion: the convective heat exchange is dominated by the air flow if the rotational speed is low, and the convective heat exchange is dominated by the rotation if the rotational speed is high.

When a TGV brakes, rotational speed and air flow velocity are connected by the relation $U=R_w\omega$. Our experimental results for this configuration show that it would be interesting to direct the air flow produced by the train displacement toward the disk. However, the air flow velocity range tested for this configuration is limited (U ranging between 8 and 12 m s^{-1}). In the future, the air flow velocity range will be increased to obtain correlations between the local Nusselt number Nu, the rotational Reynolds number Re, and the air flow Reynolds number Re_0.

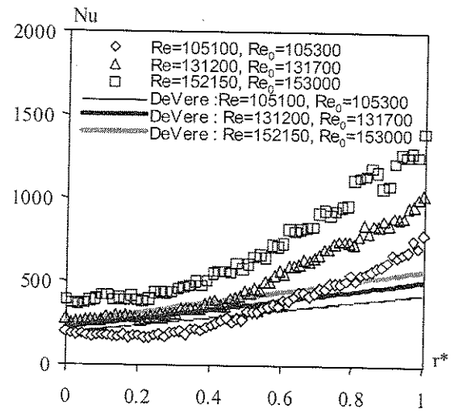

Fig. 9 The local Nusselt number as a function of the dimensionless radius for a $U=R\omega$ configuration.

References

1. B. Watel, S. Harmand, and B. Desmet, "Influence of convective heat exchange on a rotating disc in superimposed air flow—comparison

between heat pipe and solid discs," *J. Enhanced Heat Transfer* **7**, 259–272 (2000).
2. T. Von Karman, "Über laminare und turbulente Reibung," *Z. Angew. Math. Mech.* **1**, 244–252 (1921).
3. N. Gregory, J. T. Stuart, and W. S. Walker, "On the stability of three dimensional boundary layers with application to the flow due to a rotating disk," *Philos. Trans. R. Soc. London* **A248**, 155–199 (1955).
4. E. C. Cobb and O. A. Saunders, "Heat transfer from a rotating disc," *Proc. R. Soc. London, Ser. A* **236**, 343–351 (1956).
5. C. Wagner, "Heat transfer from a rotating disc to air," *J. Appl. Phys.* **15**, 837–839 (1948).
6. E. M. Sparrow and J. L. Gregg, "Heat transfer from a rotating disc to fluids of any Prandtl number," *J. Heat Transfer* **C81**, 249–251 (1959).
7. P. D. Richardson and O. A. Saunders, "Studies of flow and heat transfer associated with rotating disc," *J. Mech. Eng.* **Sc5**, 336–342 (1963).
8. D. L. Oehlbeck and F. Erian, "Heat transfer from axisymmetric sources at the surface of a rotating disc," *Int. J. Heat Mass Transf.* **22**, 601–610 (1978).
9. J. P. Hartnett, "Heat transfer from a nonisothermal disc rotating in still air," *J. Appl. Mech.* **E81**, 672–673 (1959).
10. L. A. Dorfman, *Hydrodynamic Resistance and Heat Loss from Rotating Solids*, Oliver and Boyd, Edinburgh and London (1963).
11. A. P. De Vere, "Convective heat transfer from a rotating disc in a transverse air stream," Thesis, Univ. of Leicester (1975).
12. B. Watel, S. Harmand, and B. Desmet, "Evaluation, par thermographie infrarouge, des échanges convectifs sur un disque tournant soumis à un courant d'air parallèle à sa surface," *Rev. Gen. Therm.* **3344**, 400–401, 272–285 (1995).
13. J. F. Sacadura, *Initiation aux Transferts Thermiques*, Lavoisier, Paris (1980).
14. B. Eyglument, *Manuel de Thermique*, Editions Hermes, Paris (1997).
15. D. Pajani, *Mesure par Thermographie Infrarouge*, ADD Editeur, Paris (1989).
16. G. Gaussorgues, *La Thermographie Infrarouge—Principe, Technologie, Applications*, Troisième Edition, Lavoisier (1989).
17. B. Watel, "Etude des échanges convectifs sur un cylindre ailéte en rotation, soumis à un courant d'air parallèle aux ailettes," Thèse, Univ. de Valenciennes (1997).

Monica Siroux is an assistant professor in the Science and Technology Institute of University of Valenciennes and Hainaut Cambresis (UVHC), France, where she teaches thermodynamics and heat transfer. She received her Doctor of Science degree in 1996 from the University of Paris XII. Her research topic in the Laboratory of Mechanics and Energetics of UVHC relate to the experimental analysis using infrared thermography on the convective and radiative heat transfers applied to braking systems. She also works on the experimental study of the flash evaporation of water.

Souad Harmand is a professor at the Laboratory of Mechanic and Energetic of the University of Valenciennes and Hainaut Cambraisis. She obtained her Doctor of Science degree in 1990. She is also a teacher at the Higher National School of Engineering in Mechanic and Energetic of Valenciennes. The strong points of her research relate to the development of experimental methods for the study of local convective heat transfer in the presence of complex flows. She is also interested in the development of new cooling technologies of complex machines, such as disks of brakes cooled by heat pipes and convection, or the cooling of alternators intended to equip windmills. She also works on the flash evaporation of water.

Bernard Desmet has been a professor at the University of Valenciennes and Hainaut-Cambrésis, France, since 1990, and is the director of the Laboratory of Mechanics and Energetics (LME). The dominating objective of the LME is the control and the optimization of heat and mass transfer phenomena. He leads the research group in energetics of the LME, which specializes in the thermal transfers by convection on fixed or mobile walls in the presence of complex flows. He takes part in the activities of the Pôle Frein, a research group in braking setup in the North-Pas de Calais in France, since its creation in 1990. He belongs to the executive board and the scientific council of the Pôle Frein and was president of the scientific council from 1995 to 1997.

Wavefront fitting of interferograms with Zernike polynomials

Bo Qi
Hongbin Chen, MEMBER SPIE
Nengli Dong
Chinese Academy of Sciences
Institute of Optics and Electronics
P.O. Box 350
Chengdu, Sichuan, 610209
China
E-mail: boqi@aresoft.com

Abstract. We introduce an algorithm for wavefront fitting of interferograms with Zernike polynomials. The algorithm is based on a singular value decomposition (SVD). SVD is superior to other reconstruction algorithms to some extent. We also introduce the optimum Zernike mode number. With the optimum number of modes, wavefronts can be expressed more exactly. The F-test has been widely used in many fields, and we introduce it to optical wavefront analyzing. We also do computer simulations of this algorithm. [DOI: 10.1117/1.1481726]

Subject terms: wavefront fitting; Zernike polynomials; singular value decomposition; F-test.

Paper 010125 received Apr. 9, 2001; revised manuscript received Jan. 29, 2002; accepted for publication Jan. 31, 2002.

1 Introduction

There are many classical algorithms for wavefront fitting of interferograms using Zernike polynomials[1]: the least-squares method, the Gram-Schmidt method, and the covariance matrix method. We introduce an algorithm with singular value decomposition (SVD). The stability of SVD is very good when there are more testing data than the unknown coefficients, or the matrix is singular; with SVD a satisfactory solution is always obtained. Solving the coefficients of Zernike polynomials avoids the computational error introduced by direct constructing normal equation groups. And it works well when the noise amplitude is large.

The key problem of wavefront fitting is how to express exactly the whole wavefront. In most interferogram analyzing software, the mode number for reconstruction is fixed. When analyzing high spatial frequency aberrations, the analyzed result is not accurate. To better this status, we introduce the optimum number of modes. We aim to obtain the optimum number of modes for wavefront fitting using the F-test and the condition number of the matrix.

In Sec. 1, we introduce the wavefront fitting with Zernike polynomials. In Sec. 2, we describe the test of the polynomial mode number with the F-test. In Sec. 3, we do the computer simulation of this algorithm. In Sec. 4, we give a summary.

2 Zernike Polynomials and Wavefront Fitting

Wavefront fitting's purpose is to expand a wavefront phase into a set of series in whole apertures. Using the metrical data to solve the coefficients of different modals, it achieves the expression of a full wavefront.[2] To do so, one requires that the set of series obey the following properties: it is an orthogonal system over the area of interest; and it has to be complete in the sense that any function can be approximated by linear combinations of the series with any degree of accuracy. We usually use the Zernike polynomials for their properties.[3] Zernike polynomials are a product of radial polynomials and triangular functions as

$$Z_i(r,\theta)=R_n^m(r)\Theta^m(\theta), \tag{1}$$

where the radial polynomials are defined as

$$R_n^m(r)=\sum_{s=0}^{(n-m)/2}\frac{(-1)^s\sqrt{n+1}(n-s)!r^{n-2s}}{s![(n+m)/2-s]![(n-m)/2-s]!} \tag{2}$$

and the triangular function as

$$\Theta^m(\theta)=\begin{cases}\sqrt{2}\cos m\theta & m\neq 0 \quad m \text{ is even}\\ \sqrt{2}\sin m\theta & m\neq 0 \quad m \text{ is odd}\\ 1 & m=0\end{cases}. \tag{3}$$

The radial degree n and the azimuthal frequency m should satisfy $m\leqslant n$ and $n-m=$ even. The index i orders the polynomials. For a given n, terms with lower values of m are ordered first. Table 1 shows our numbering of the polynomials used.

Any wavefront function can be expanded into the linear combinations of P polynomials,

$$w(x,y)=\sum_{i=1}^{P}k_iZ_i(x,y), \tag{4}$$

where Z_i denotes the i'th Zernike polynomial, while k_i is the coefficient.

Giving N discrete data points $w_i(x_i,y_i)$, $i=1,2,...,N$. Rewrite Eq. (4) in compact form as:

$$\mathbf{W}=\mathbf{ZK}, \tag{5}$$